Integration of Capacitive and Piezoelectric Accelerometers Using a Digital Approach

Yu-Sheng Lu and Po-Chen Lee
Department of Mechatronic Engineering, National Taiwan Normal University, Taipei 106, Taiwan
Email: luys@ntnu.edu.tw; jackylee0526@gmail.com

***Abstract*—This study is to obtain an acceleration signal with a nice quality and apply it to a linear motion stage. The accelerometers used in this paper are piezoelectric and capacitive accelerometers. Since a piezoelectric accelerometer cannot measure low-frequency acceleration, its application to servo systems is limited. On the contrary, a capacitive accelerometer is able to measure low-frequency acceleration. However, its output noise is significant, and its dynamic bandwidth is small compared with the piezoelectric accelerometer. This paper proposes a high-performance accelerometer, which digitally integrates the salient features of both capacitive and piezoelectric accelerometers. The proposed accelerometer can measure both low- and high-frequency acceleration. It is also applied to compensating for load disturbance in a linear drive for performance improvement.**

***Index Terms*—capacitive accelerometer, digital integration, motion control, piezoelectric accelerometer**

I. Introduction

In recent years, the application of accelerometers has become ubiquitous. The studies [1]-[4] use acceleration signals to facilitate velocity estimation, which improves tracking performance of servo systems. Accelerometers have been used to measure vehicle braking deceleration for assessing road surface friction, based on a Raspberry-Pi single-board computer [5]. Usually, accelerometers are deployed to measure vibrations in a standard experimental setup for structural condition monitoring or damage detection [6]. As another examples, accelerometers were used to enhance feedback control laws, applied to motion control of a linear motor and a robotic arm [7], [8].

Many kinds of accelerometers have been proposed for practical applications. Among all the accelerometers, the two most popular, commonly used accelerometers are capacitive MEMS (micro-electromechanical system) and piezoelectric accelerometers [9]. Due to the rapid development of MEMS technology, capacitive accelerometers are low-cost and have high sensitivity. Generally speaking, the higher the bandwidth of the capacitive accelerometer, the larger the output noise. With similar output noise, capacitive accelerometers have much less bandwidths than piezoelectric accelerometers. The piezoelectric accelerometer possesses a broad frequency response. However, it cannot measure low-frequency acceleration, so it cannot be used in general motion control systems. In [10], the shortcomings of capacitive and piezoelectric accelerometers are improved by combining a capacitive accelerometer with a piezoelectric accelerometer using analog circuits. In this paper, a digital approach is used to fusing these two accelerometers. Compared with the analog implementation [10], the digital approach reduces implementation complexity and also provides flexibility in sensor design. In this paper, the proposed digital design is presented, and experimental results on a linear stage are reported to investigate effectiveness of the proposed approach.

Manuscript received April 29, 2019; revised June 25, 2019; accepted July 15, 2019.

Corresponding author: Yu-Sheng Lu (email: luys@ntnu.edu.tw).

II. Digitally Integrated Accelerometer

As described in the previous section, a capacitive accelerometer has the disadvantage of low bandwidths whereas the piezoelectric accelerometer has the disadvantage of being unable to measure nearly static acceleration. An analog integrated accelerometer has been proposed in [10] to obtain a high-performance accelerometer for servo applications. Fig. 1 demonstrates the structure of the analog integrated accelerometer, where a_c and a_p respectively represent the capacitive and piezoelectric accelerometers' outputs. Moreover, $H(s)$ and $L(s)$ respectively denote analog high- and low-pass filters, in which there is a design constraint, $H(s)+L(s)=1$. As shown in Fig. 1, the capacitive accelerometer's output, a_c, passes through an analog low-pass filter, whose break frequency must be higher than the minimum measurement frequency of the piezoelectric accelerometer. On the other hand, the piezoelectric accelerometer's output, a_p, is subjected to a high-pass filter, whose cutoff frequency must be less than the maximum measurement frequency of the capacitive accelerometer, so that the two signals are combined to form a complete acceleration signal. This paper proposes a digitally integrated accelerometer. Fig. 2 depicts the block diagram of the proposed digitally integrated accelerometer, in which a_i is the output of the proposed accelerometer, ADC denotes an analog-to-digital converter, and $L(z)$ is a digital low-pass filter. Compared with the analog integrated accelerometer, the proposed accelerometer reduces the required analog circuit, simplifies implementation complexity, and also improves design flexibility.

doi: 10.18178/ijeetc.8.6.346-351

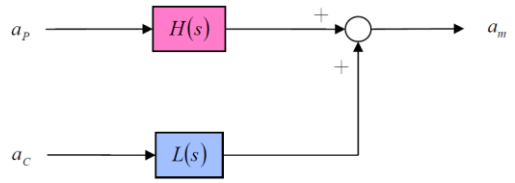

Fig. 1. Structure of the analog integrated accelerometer [10].

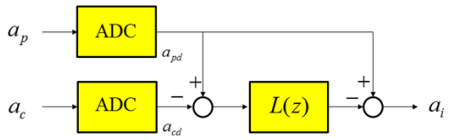

Fig. 2. The digitally integrated accelerometer.

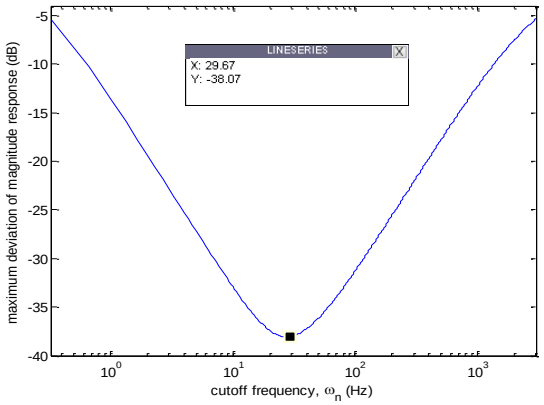

Fig. 3. Search for the optimal cutoff frequency of the low-pass filter.

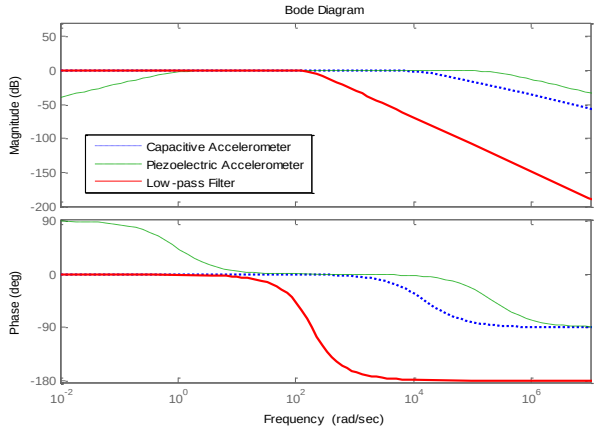

Fig. 4. Frequency response of the designed low-pass filter.

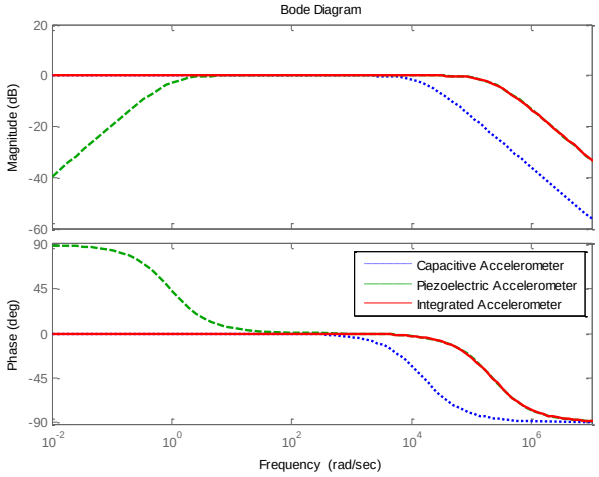

Fig. 5. Frequency responses of various accelerometers.

Design of the digital low-pass filter is the key to the proposed accelerometer. In this study, an analog second-order Butterworth filter, $L(s)$, is first determined, and $L(z)$ is then obtained by discretizing $L(s)$ using bilinear transformation with frequency prewarping. The cutoff frequency of $L(s)$ is determined to minimize the amount of maximum magnitude deviation,

$$\max \left| A_i(s) - \left[A_p(s) - L(s)\left(A_p(s) - A_c(s)\right)\right] \right|_{s=j\omega} \quad (1)$$

where $A_c(s)$, $A_p(s)$, and $A_i(s)$ are respectively the transfer functions of capacitive, piezoelectric, and desired integrated accelerometers. The amount of maximum deviation is calculated in Matlab, and the cutoff frequency of $L(s)$ is searched to give the optimal cutoff frequency of 29.67 Hz, as shown in Fig. 3. After discretizing the analog prototype, $L(s)$, and prewarping for preserving the optimal cutoff frequency, it gives:

$$L(z) = \frac{7.112\times10^{-5} z^2 + 1.422\times10^{-4} z + 7.112\times10^{-5}}{z^2 - 1.9760\, z + 0.9763} \quad (2)$$

Fig. 4 shows the frequency response of the determined optimal low-pass filter. As shown in Fig. 5, the digitally combined accelerometer is devised to improve both the bandwidth of the capacitive accelerometer and the low-frequency response of the piezoelectric accelerometer. Its frequency response is close to that of the capacitive accelerometer at low frequencies and also to that of the piezoelectric accelerometer at high frequencies.

III. Experimental System

A. Linear Motion Stage

Fig. 6 shows the experimental system that is a linear motion stage. The precision linear module consists of a ball lead screw (HIWIN KK6010P-600A1-F0) and a servo motor (HF-MP43), and the load is placed on the KK6010P stage. The position measuring sensors include an optical linear scale and a laser displacement sensor (LDS). The optical linear scale is of Carmar's WTB5-0600MM, which is connected to the precision linear module to detect the displacement of the load on the lead screw. The LDS is of MTI Instruments' LTC-025-04-SA, and it is used for absolute position measurement.

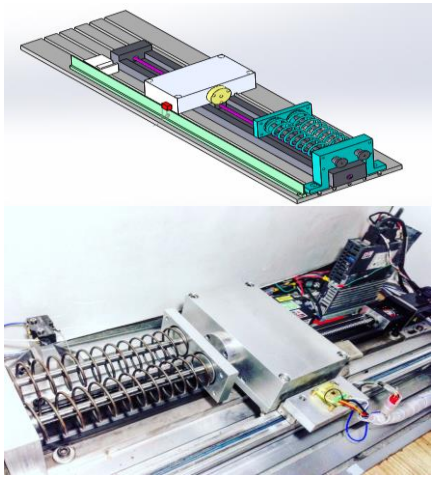

Fig. 6. Experimental system.

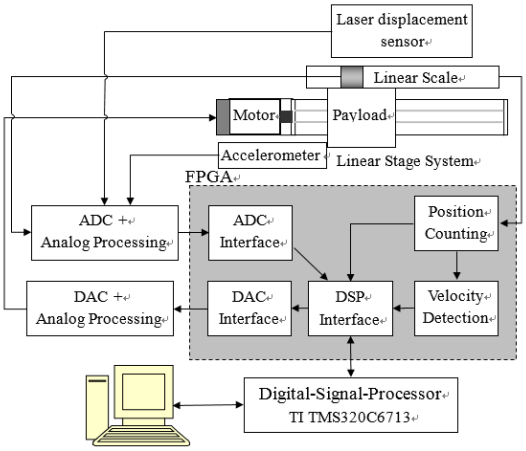

Fig. 7. Schematic of the experimental system.

Fig. 7 shows the schematic of the experimental system. The optical scale provides the A- and B-phase signals to the quadruple frequency circuit implemented in the FPGA. The quadruple frequency circuit increases accuracy of position measurement by 4 times to 5 μm. To have the same initial position for each experiment, the LTC-025-04-SA LDS with a resolution of 0.5 μm is used to adjust the initial position of payload. The piezoelectric accelerometer used in this experiment is 333B50 from PCB Piezotronics Inc., with an output sensitivity of 1000 mV/g, a peak-to-peak measurement range of ±5g, and a measurement frequency range from 0.15 Hz to 3500 Hz [11]. In this paper, the desired transfer function of the integrated accelerometer, $A_i(s)$, is assigned to be of first order and have unity *dc* gain and an edge frequency equal to the upper band-edge frequency of the piezoelectric accelerometer. The capacitive accelerometer used in this experiment is a two-axes ADXL325 accelerometer from Analog Devices Inc. Its sensitivity is 174 mV/g, the peak-to-peak range is also ±5g, and the maximum bandwidth is 1.6 kHz [12]. Hence, the capacitive accelerometer is modeled as a first-order transfer function, $A_c(s)$, having unity *dc* gain and a cutoff frequency of $2\pi\times1600$ rad/s.

The DSP reads the position count from the FPGA and uses the Finite-Difference Method (FDM) [13] for velocity estimation in the following experiments. The interrupt frequency for the DSP interrupt service routine is 10.986 kHz. For more details about the experimental system, please refer to [14].

B. Controller Design

The dynamic model of the experimental system is identified using a dynamic signal analyzer (DSA) and is described by:

$$m_0\ddot{x} + B_0\dot{x} = G(u + d) \tag{3}$$

where G=41600, m_0=28.1271, B_0=23.1598, d denotes an unknown disturbance, x is the position of payload, and u is the input to the plant. Consider a positional reference, r, which is assumed to be twice differentiable. Moreover, define the tracking error, $e = x - r$. Let a position controller be designed as:

$$u = G^{-1}\left\{B_0 x + m_0\left[\ddot{r} - M_r^{-1}(B_r\dot{e} + K_r e)\right]\right\} - \hat{d} \tag{4}$$

where M_r, B_r, and K_r are respectively the desired mass, damping, and spring coefficients, and $\hat{d}$ denotes a disturbance estimate. Here, the disturbance estimate, $\hat{d}$, is produced by an acceleration-based disturbance observer (ADOB) [14].

The ADOB receives an acceleration signal from an accelerometer and generates a disturbance estimate, $\hat{d}$, for disturbance compensation. In this paper, various accelerometers are evaluated by sending their outputs to ADOBs to generate corresponding disturbance estimates. However, only one disturbance estimate at a time is used for disturbance compensation to improve positional tracking precision. The accelerometer that gives the best positional tracking performance is considered superior to others. To evaluate tracking performance, the following performance indices [15] are defined:

$$\text{IAE}_e = \int_0^T |e(t)|\,dt\,,\quad \text{CI}_e = \frac{1}{T}\int_0^T |e(t) - \bar{e}(t)|\,dt$$

$$\text{CI}_u = \frac{1}{T}\int_0^T |u(t) - \bar{u}(t)|\,dt \tag{5}$$

where T denotes the final time in an experiment, $\bar{e}(t)$ denotes the filtered position error, and $\bar{u}(t)$ is the filtered control amount. The filter is designed using Matlab's *butter* function with a filter bandwidth of 50Hz, and the filter is performed using the Matlab's *filtfilt* function. In the following closed-loop control experiments, the following parameters are chosen: M_r=m_0, B_r=2×25M_r, and K_r=25^2M_r. Moreover, the filter in the ADOB is chosen to be of first order and with a cutoff frequency of 15 Hz.

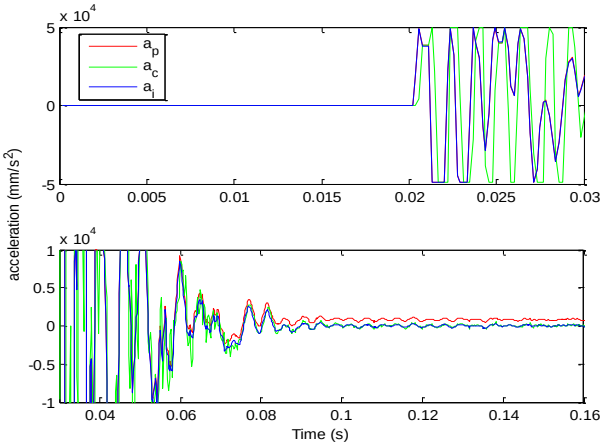

Fig. 8. Responses of various accelerometers to a shock disturbance.

IV. Experimental Results

A. Open-Loop Experiment

The control effort in the open loop experiment is 0 V, the load is still at its original position, and then a shock disturbance is applied to the load at 0.02 s. Fig. 8 shows the corresponding outputs of various accelerometers. From the upper subplot of Fig. 8, it is seen that the piezoelectric accelerometer's output leads the capacitive

accelerometer's output at high frequencies. Moreover, both the piezoelectric and the proposed accelerometers have similar outputs at high frequencies. From the lower subplot of Fig. 8, it is seen that the capacitive accelerometer's response is similar to the proposed accelerometer's output after about 0.08 s. It also demonstrates that the piezoelectric accelerometer is unable to measure low-frequency acceleration.

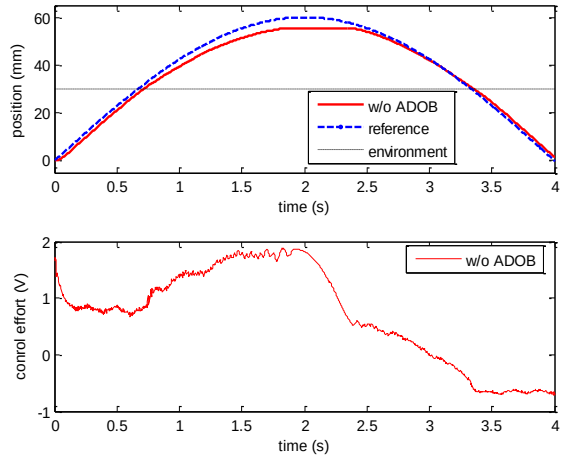

Fig. 9. Sinusoidal response without disturbance compensation.

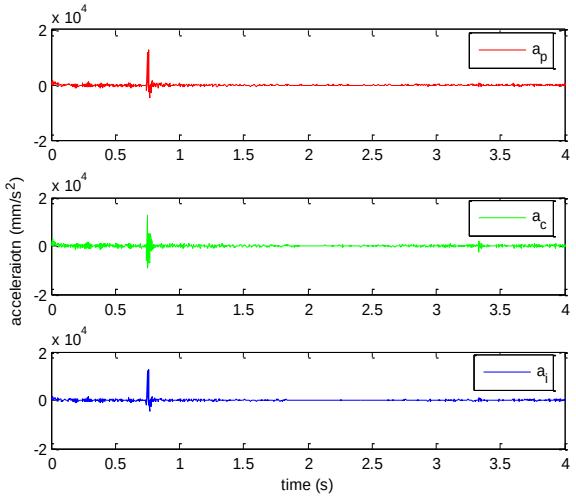

Fig. 10. Accelerometer outputs during a sinusoidal response without disturbance compensation.

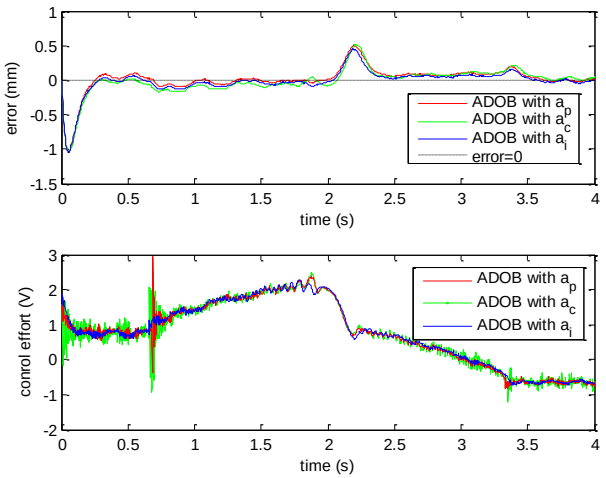

Fig. 11. Sinusoidal responses with disturbance compensation.

B. Tracking Control Experiments

Consider two reference commands. They are a sinusoidal reference, $r = 60\sin(\pi t/4)\,(\text{mm})$, and a minimum-jerk reference,

$$\begin{aligned} r = {} & \ell\left[10t^3 - 15t^4 + 6t^5\right]\left(H(t) - H(t-1)\right) \\ & + \ell\left[1 + 10(t-1)^3 - 15(t-1)^4 + 6(t-1)^5\right]\left(H(t-1) - H(t-2)\right) \\ & + \ell\left[1 + 10(3-t)^3 - 15(3-t)^4 + 6(3-t)^5\right]\left(H(t-2) - H(t-3)\right) \\ & + \ell\left[10(4-t)^3 - 15(4-t)^4 + 6(4-t)^5\right]\left(H(t-3) - H(t-4)\right), \end{aligned} \tag{6}$$

where $\ell = 30$ (mm), and $H(\cdot)$ represents the Heaviside function. Fig. 9 shows the sinusoidal response without disturbance compensation. Fig. 10 shows corresponding outputs of various accelerometers, demonstrating that output responses of all accelerometers have similar oscillations in this experiment without disturbance compensation. Fig. 11 shows sinusoidal responses with disturbance compensation based on the same ADOB. Moreover, Fig. 12 shows corresponding outputs of various accelerometers. It is seen that the capacitive accelerometer's output becomes much oscillatory compared with the one in the experiment without disturbance compensation shown in Fig. 10. Fig. 12 also demonstrates that the proposed and the piezoelectric accelerometers produce less oscillations than the capacitive accelerometer. Table I gives performance indices for sinusoidal responses with disturbance compensation, showing that the proposed accelerometer produces better performance than the other accelerometers in terms of IAE and CI.

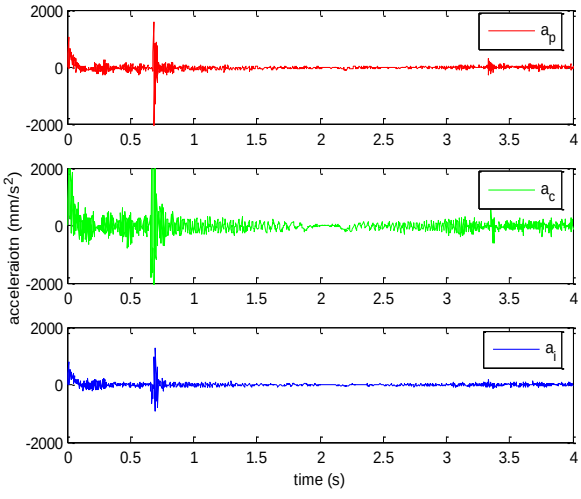

Fig. 12. Accelerometer outputs during sinusoidal responses with disturbance compensation.

TABLE I. PERFORMANCE INDICES FOR SINUSOIDAL RESPONSES WITH DISTURBANCE COMPENSATION

Parameter	IAE$_e$ (mm·s)	CI$_e$ (mm)	CI$_u$ (V)
a_p	0.3939	0.00618	0.0490
a_c	0.4621	0.00642	0.1062
a_i	0.3690	0.00561	0.0456

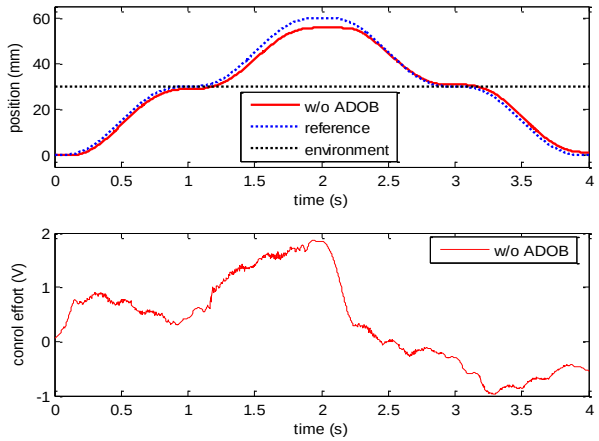

Fig. 13. Minimum-jerk response without disturbance compensation.

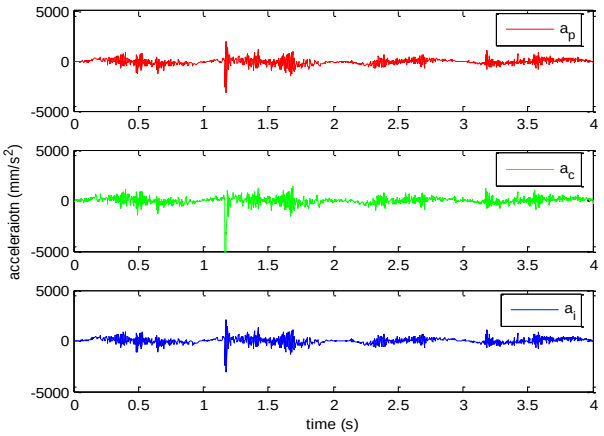

Fig. 14. Accelerometer outputs during a minimum-jerk response without disturbance compensation.

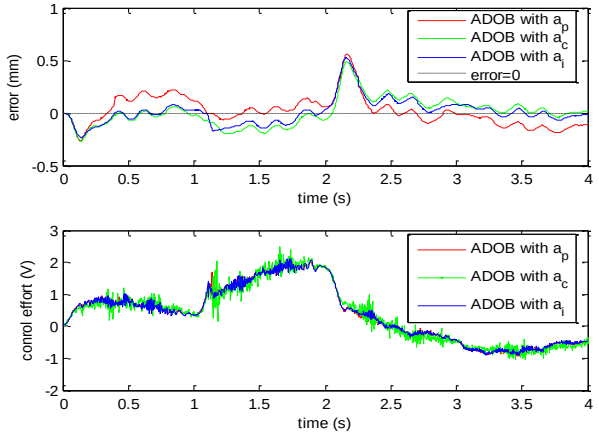

Fig. 15. Minimum-jerk responses with disturbance compensation.

Fig. 13 shows the response subject to a minimum-jerk reference without disturbance compensation. Fig. 14 shows the corresponding responses of various accelerometers, in which all three accelerometers produces similar amounts of oscillations in their outputs. Fig. 15 shows the minimum-jerk responses with disturbance compensation based on the same ADOB. Fig. 16 shows the corresponding outputs of accelerometers. Likewise, the capacitive accelerometer produces a more oscillatory output than both the piezoelectric and the proposed accelerometers. Table II gives performance indices for those responses shown in Fig. 15, showing that compared with the other two accelerometers, the proposed accelerometer not only produces the smallest tracking error and also gives the smoothest response.

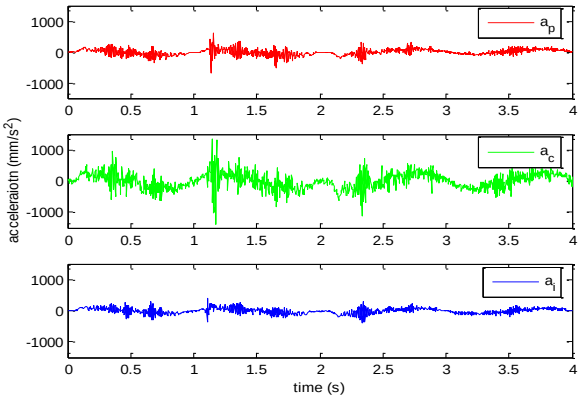

Fig. 16. Accelerometer outputs during minimum-jerk responses with disturbance compensation.

TABLE II. PERFORMANCE INDICES FOR MIN.-JERK RESPONSES WITH DISTURBANCE COMPENSATION

Parameter	IAE_e (mm·s)	CI_e (mm)	CI_u (V)
a_p	0.4146	0.0024	0.0314
a_c	0.4046	0.0042	0.0791
a_i	0.3376	0.0023	0.0281

V. CONCLUSIONS

This paper has proposed a digitally integrated accelerometer that combines capacitive and piezoelectric accelerometers using ADCs and digital systems. The digitally integrated accelerometer simplified the required analog sensor circuitry and also provides the flexibility in sensor integration. Experimental results on a linear motion stage demonstrate that the proposed accelerometer can give accurate tracking performance using smooth control efforts compared with the capacitive and the piezoelectric accelerometers.

ACKNOWLEDGMENT

This work was supported in part by the Ministry of Science and Technology under Grants No. MOST 107-2221-E-003-021.

REFERENCES

[1] S. Jeon and M. Tomizuka, "Benefits of acceleration measurement in velocity estimation and motion control," *Control Engineering Practice*, vol. 15, no. 3, pp. 325–332, 2007.

[2] J. C. Zheng and M. Y. Fu, "A reset state estimator using an accelerometer for enhanced motion control with sensor quantization," *IEEE Trans. Contr. Syst. Technol.*, vol. 18, no. 1, pp. 79-90, 2010.

[3] W. H. Zhu and T. Lamarche, "Velocity estimation by using position and acceleration sensors," *IEEE Trans. Ind. Electron.*, vol. 54, no. 5, pp. 2706–2715, Oct. 2007.

[4] Y. S. Lu and C. H. Lee, "Experimental evaluation of acceleration-enhanced velocity estimation algorithms using a linear motion stage," *Journal of the Brazilian Society of Mechanical Sciences and Engineering*, vol. 39, no. 2, pp. 543–551, Feb. 2017.

[5] M. Ambrož, U. Hudomalj, A. Marinšek, and R. Kamnik, "Raspberry Pi-based low-cost connected device for assessing road surface friction," *Electronics*, vol. 8, no. 3, pp. 341-356, 2019.

[6] R. Janeliukstis, "Review on time-frequency-based machine learning for structural damage assessment and condition monitoring," in *Proc. 18th Int. Scientific Conf. Engineering for Rural Development*, May 2019.

[7] K. K. Tan, S. Y. Lim, T. H. Lee, and H. Dou, "High-precision control of linear actuators incorporating acceleration sensing," *Robotics and Computer-Integrated Manufacturing*, vol. 16, no. 5, pp. 295–305, Oct. 2000.

[8] W. L. Xu and J. D. Han, "Joint acceleration feedback control for robots: Analysis, sensing and experiments," *Robotics and Computer-Integrated Manufacturing*, vol. 16, no. 5, pp. 307–320, Oct. 2000.

[9] G. D'Emilia, A. Gaspari, and E. Natale, "Amplitude–phase calibration of tri-axial accelerometers in the low-frequency range by a LDV," *J. Sens. Sens. Syst.*, vol. 8, pp. 223–231, May 2019.

[10] Y. S. Lu, H. W. Wang, and S. H. Liu, "An integrated accelerometer for dynamic motion systems," *Measurement*, vol. 125, pp. 471–475, Sep. 2018.

[11] *Model 333B50 Installation and Operating Manual*, PCB Piezotronics Inc., NY, U.S.A., 2002.

[12] *ADXL325: Small, Low Power, 3-Axis ±5 g Accelerometer Data Sheet*, Analog Device Inc., MA, U.S.A., 2009.

[13] L. Bascetta, G. Magnani, and P. Rocco, "Velocity estimation: assessing the performance of non-model-based techniques," *IEEE Trans. Control Systems Technology*, vol. 17, no. 2, pp. 424–433, 2009.

[14] Y. S. Lu and S. H. Liu, "The design and implementation of an accelerometer-assisted velocity observer," *ISA Trans.*, vol. 59, pp. 418–423, Nov. 2015.

[15] M. M. Abdelhameed, "Enhancement of sliding mode controller by fuzzy logic with application to robotic manipulators," *Mechatronics*, vol. 15, no. 4, pp. 439–58, 2005.

Yu-Sheng Lu received the B.S. degree in mechanical and electrical engineering from National Sun Yat-Sen University, Kaohsiung, Taiwan, in 1990, and the Ph.D. degree in engineering from National Tsing Hua University, Hsinchu, Taiwan, in 1995.

From 1997 to 1998, he was at the Opto-Electronics & Systems Laboratories, ITRI, Taiwan. From 1998 to 2000, he was with the Institute of Robotics and Mechatronics, DLR, Germany. From 2000 to 2008, he was with the Department of Mechanical Engineering, National Yunlin University of Science and Technology, Yunlin, Taiwan. In 2008, he moved to the Department of Mechatronic Engineering, National Taiwan Normal University, Taipei, Taiwan, where he is currently a professor. His research interests include control system design with applications to mechatronic systems.

Po-Chen Lee received the M.S. degree in mechatronic engineering from National Taiwan Normal University, Taipei, Taiwan, in 2017.